Biosensors and Bioelectronics ■ (■■■■) ■■■–■■■

Contents lists available at ScienceDirect

Biosensors and Bioelectronics

journal homepage: www.elsevier.com/locate/bios

A reusable magnetic graphene oxide-modified biosensor for vascular endothelial growth factor detection in cancer diagnosis

Chih-Wen Lin [a,1], Kuo-Chen Wei [b,1], Shih-sheng Liao [a], Chiung-Yin Huang [b], Chia-Liang Sun [c], Pei-Jung Wu [a], Yu-Jen Lu [b], Hung-Wei Yang [d,*], Chen-Chi M. Ma [a,**]

[a] Department of Chemical Engineering, National Tsing Hua University, 101, Section 2, Kuang-Fu Road, Hsinchu 30013, Taiwan, ROC
[b] Department of Neurosurgery, Chang Gung Memorial Hospital, Linkou, 5 Fu-shing Road, Kuei-Shan, Tao-Yuan 33305, Taiwan, ROC
[c] Department of Chemical and Materials Engineering, Chang Gung University, 259 Wen-Hwa 1st Road, Kuei-Shan, Tao-Yuan 33302, Taiwan, ROC
[d] Institute of Medical Science and Technology, National Sun Yat-sen University, Kaohsiung 80424, Taiwan, ROC

ARTICLE INFO

Article history:
Received 5 June 2014
Received in revised form
12 August 2014
Accepted 27 August 2014

Keywords:
Magnetic graphene oxide (MGO)
Vascular endothelial growth factor (VEGF)
Reusable biosensor
Differential pulse voltammetry (DPV)
Cancer diagnosis

ABSTRACT

Early cancer diagnosis is critical for the prevention of metastasis. However, simple and efficient methods are needed to improve the diagnosis and evaluation of cancer. Here, we propose a reusable biosensor based on a magnetic graphene oxide (MGO)-modified Au electrode to detect vascular endothelial growth factor (VEGF) in human plasma for cancer diagnosis. In this biosensor, Avastin is used as the specific biorecognition element, and MGO is used as the carrier for Avastin loading. The use of MGO enables rapid purification due to its magnetic properties, which prevents the loss of bioactivity. Moreover, the biosensor can be constructed quickly, without requiring a drying process, which is convenient for proceeding to detection. Our reusable biosensor provides the appropriate sensitivity for clinical diagnostics and has a wide range of linear detection, from 31.25–2000 pg mL^{-1}, compared to ELISA analysis. In addition, in experiments with 100% serum from clinical samples, readouts from the sensor and an ELISA for VEGF showed good correlation within the limits of the ELISA kit. The relative standard deviation (RSD) of the change in current (ΔC) for reproducibility of the Au biosensor was 2.36% ($n=50$), indicating that it can be reused with high reproducibility. Furthermore, the advantages of the Avastin-MGO-modified biosensor for VEGF detection are that it provides an efficient detection strategy that not only improves the detection ability but also reduces the cost and decreases the response time by 10-fold, indicating its potential as a diagnosis product.

1. Introduction

Angiogenesis is closely related to tumor growth and metastasis (Carmeliet and Jain, 2000; Hanahan and Folkman, 1996). Vascular endothelial growth factor (VEGF) is an important growth factor that regulates the progression angiogenesis, both physiologically and pathologically (Ferrara et al., 2003; Jain, 2003; Laguens et al., 2006). In addition, VEGF overexpression appears in many human cancers, such as brain tumors (Bando et al., 2004; Cheng et al., 1996), lung cancer (Kaya et al., 2004), breast cancer (Carmeliet and Jain, 2000; Hanahan and Folkman, 1996), gastrointestinal cancer (Aoyagi et al., 2005) and urinary tract tumors (Wu et al., 2003). Avastin is a potential candidate for the development of anti-angiogenic drugs against VEGF (Wu et al., 2008), which is also a humanized anti-VEGF antibody (Wang et al., 2004). Thus, it is recognized as an extremely potent angiogenesis inhibitor instead of VEGF-antibody due to its specificity for VEGF (Hsu et al., 2014). It is a critical and challenging task to develop faster, selective and sensitive methods for the detection of VEGF in the serum of patients for early disease diagnosis and efficient therapeutic monitoring strategies.

Electrochemical biosensors convert chemical signals into a measurable amperometric signal using potentiometric, amperometric and impedimetric transducers to simultaneously detect and analyze a specific compound of interest. In 1962, the first enzyme electrode was introduced using glucose oxidase immobilization (Clark and Lyons, 1962). Currently, various biosensor devices have been developed and are commercially produced for a wide range of applications, with blood glucose detection being especially important for diabetes. Enzyme-based electrochemical biosensors

* Corresponding author.
** Corresponding author. Fax: +886 3 5715408.
E-mail addresses: howardyang@mail.nsysu.edu.tw (H.-W. Yang), ccma@che.nthu.edu.tw (C.-C. Ma).
[1] These authors contributed equally to this work.

http://dx.doi.org/10.1016/j.bios.2014.08.080
0956-5663/

can be used as labels bound to antibodies, antigens or oligonucleotides with a specific sequence, providing affinity-based sensors (Jain, 2003) for the monitoring of clinically important metabolites. The most common enzyme labels for electrochemical affinity biosensors are peroxidase and alkaline phosphatase (Kauffmann and Guilbault, 1991). Recently, various biomarkers have been used in electrochemical affinity biosensors, including emerging cancer biomarkers. Gang-Il Kim reported VEGF as a cancer-related biomarker for monitoring angiogenesis and metastasis with gold nanoparticles (Au-NPs), which were self-assembled onto an indium tin oxide (ITO) electrode to prepare a modified sandwich-type electrochemical immunoassay platform. In this sensor, the amperometric signal was measured by the differential pulse voltammetry (DPV), which increased almost linearly from 1.27×10^{-4} to 4.17×10^{-4} A with increasing concentrations of VEGF from 100 to 600 pg mL^{-1} (Kim et al., 2010). A high-performance VEGF biosensor using p-type field-effect transistor (FET) sensor was reported (Kwon et al., 2010). This FET biosensor could display near 400 fM of VEGF concentration in real-time by investigated current–voltage (*I*–*V*) curve. Feasibility for the detection of VEGF in the serum of patients has been reported. VEGF can be directly detected in 50% blood serum, and the lowest detection limit reached was 190 pg mL^{-1} (Zhao et al., 2011). Furthermore, biosensors have the potential to provide a rapid, selective, sensitive, lower cost and simplified measurement technology in the clinic compared to the ELISA method.

Graphene is a multi-functional material that has been modified and widely used in biomedical applications, including drug delivery (Lu et al., 2012), cancer therapy (Yang et al., 2013b, 2013c), and biosensors (Li et al., 2013). Kuila overviewed the recent advances in graphene-based electrochemical biosensors (Kuila et al., 2011) and summarized their many advantages, which include a large surface area, excellent electrical conductivity, rapid electron transfer and selective biomolecule detection. However, graphene has rarely been applied in the cancer biomarker field. Although Zhang et al. investigated the feasibility of graphene films as flexible VEGF biosensor had capable of detecting VEGF as low as 1 pg/mL by measured the resistance changes curve (Zhang et al., 2013), but there were not enough electrochemical data to evaluate the potential of detection used real sample. Besides, graphene based sensors has been mainly used for the detection of glucose, cytochrome c, nicotinamide adenine dinucleotide, hemoglobin, cholesterol, ascorbic acid (AA), uric acid (UA), dopamine (DA), and hydrogen peroxide (H_2O_2). Magnetic graphene oxide (MGO) is prepared through the in situ generation and deposition of Fe_3O_4 nanoparticles onto the surface of graphene oxide. Teymourian investigated the synergistic integration of these two nano-materials on the electrocatalytic behavior of different important electroactive compounds (Teymourian et al., 2013). Additionally, a simple, cheap, stable, reusable, highly selective and sensitive amperometric assay to detect H_2O_2 and glucose in buffer solution and diluted blood samples has been reported (Yang et al., 2013a). Both of these studies demonstrate that the excellent electrocatalytic activity of MGO could be promising for the development of electrochemical biosensors.

Here, we developed a rapid, simple and reusable strategy for detecting the VEGF concentration in human serum using an Avastin-MGO-modified Au electrode. First, Avastin, which contains VEGF antibody fragments, was conjugated onto the surface of MGO by EDC/NHS chemistry to form an Avastin-MGO stock solution. Second, the Avastin-MGO stock solution was drop-deposited firmly to the sensing area of a Au electrode under a magnetic field during VEGF detection. The amperometric signal was measured by differential pulse voltammetry (DPV) to quantify the VEGF concentration. Finally, the practical utility of the proposed biosensor was evaluated by determining the VEGF levels in human serum samples from both healthy people and patients with brain tumors. The developed reusable biosensor is simple, sensitive, specific, fast and stable for the detection of VEGF, a predominant biomarker of cancer angiogenesis.

2. Materials and methods

2.1. Synthesis of Avastin-MGO

The synthesis procedure is described in Scheme 1A. GO was prepared from nano-graphite platelets (NGPs) powders by the modified Hummers' method (Stankovich et al., 2006, 2007). MGO composites were synthesized by coprecipitation of $FeCl_3\cdot6H_2O$ and $FeCl_2\cdot4H_2O$ in the presence of GO powder. An aqueous suspension of MGO was sonicated for approximately 15 min to prepare Avastin-MGO, which was subsequently used to cover the Au electrode in this study. Twenty-seven milligrams of sulfo-NHS and 24 mg of EDC · HCl were dissolved in 2 mL of 0.5 M MES buffer (pH=6.3) in the dark. A 0.1 mL aliquot of this solution was mixed with 0.05 mL of MGO (10 mg mL^{-1}) at 25 °C and reacted for 30 min in the dark to activate the carboxyl groups of MGO. Activated MGO was separated, washed with 0.8 mL of 0.1 M MES buffer, resuspended in 150 μL of MES buffer, and then mixed with 500 μg mL^{-1} of Avastin at 25 °C by vortexing for 1 h followed by sonication for 1 h. The primary amino groups of Avastin reacted with the active ester, resulting in covalent conjugation of Avastin to the surface of MGO. The Avastin-MGO was then separated from the solution, washed with DI water to remove the MES buffer and unbound Avastin, and dispersed in 0.1 mL of DI water. The binding capacity was analyzed by Ultraviolet–visible spectroscopy (UV–vis, Heliosα, Thermo) at 279 nm.

2.2. VEGF detection by the Avastin-MGO-modified Au electrode

Scheme 1B shows the process of electrochemical detection by the Avastin-MGO-modified Au electrode in 1 mM ($K_3[Fe(CN)_6]$)/($K_4[Fe(CN)_6]$), and 0.1 M KCl solution was to establish the baseline current before any samples were measured. For the VEGF standard curve, 15 μL of various concentrations of VEGF solution was pipetted onto the surface of the Avastin-MGO-modified Au electrode and incubated for 30 min. The plasma samples were prepared from human as follows: the plasma was collected from a whole blood sample (10 mL) using heparin as an anticoagulant and centrifuged for 15 min at 3500 rpm and 4 °C for 15 min, and the supernatant (plasma) was collected for VEGF detection. This study was approval by institutional review board (IRB: CGMH 101-0430C). The concentrations of VEGF were calculated using the respective calibration curves for the electrochemical sensing and ELISA assays.

3. Results and discussion

3.1. Characterization of GO and MGO

The average sheet sizes of GO and MGO were approximately 1.5 and 3 μm (Fig. 1A), as determined by transmission electron microscopy (TEM). Closer examination revealed that Fe_3O_4 was attached to the surface of MGO sheets and exhibited a sphere-like morphology with an approximate size of 7–12 nm (Fig. 1A). Atomic force microscopy (AFM) images showed that the thicknesses and roughness of GO and MGO (Fig. S1A and B). X-ray photoelectron spectroscopy (XPS). The GO sample showed C1s and O1s peaks at 285 eV and 532 eV, respectively (Fig. S2A and B). Additionally, XPS (C1s) of GO was used to characterize the main functional groups

Please cite this article as: Lin, C.-W., et al., Biosensors and Bioelectronics (2014), http://dx.doi.org/10.1016/j.bios.2014.08.080

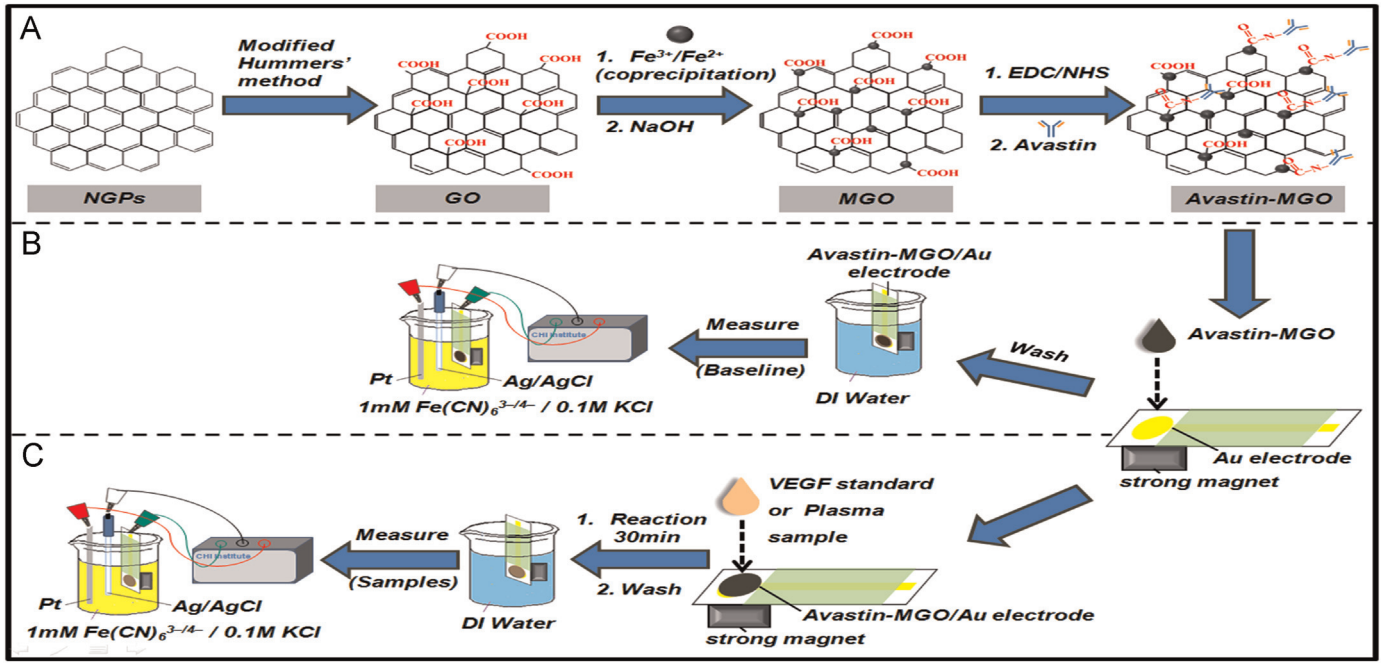

Scheme 1. (A) Synthesis of Avastin-MGO. (B) Electrochemical detection by Avastin-MGO/Au. (C) Electrochemical detection of VEGF in samples using the Avastin-MGO/Au sensor.

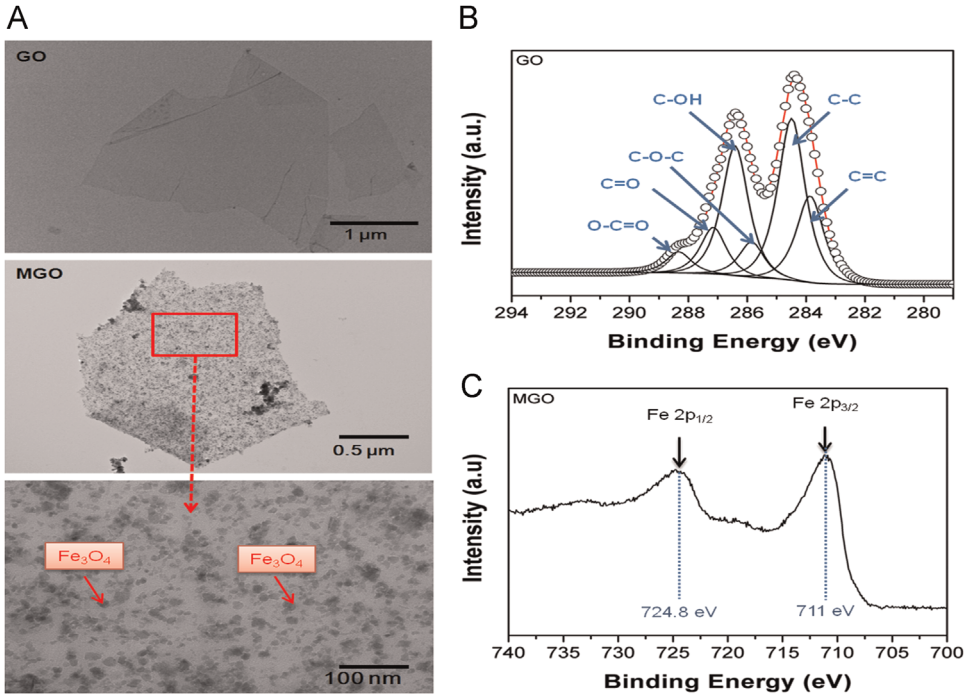

Fig. 1. (A) TEM images showing the morphologies of GO (top) and MGO (middle). An enlarged image of the red area from MGO is also shown (bottom). (B) XPS C 1s peaks of GO. (C) XPS Fe 2p peaks of MGO. (For interpretation of the references to color in this figure legend, the reader is referred to the web version of this article.)

on GO. The peaks observed at 284.2, 284.8, 286.1, 286.6, 287.4, and 288.6 eV were assigned to carbon atoms in C=C, C–C, C–OH, C–O–C, C=O and O–C=O, respectively (Fig. 1B) (Yang et al., 2011). The Fe 2p peaks of MGO located at 711 and 724.8 eV corresponded to Fe $2p_{3/2}$ and Fe $2p_{1/2}$ (Liu et al., 2009), respectively (Fig. 1C), and their presence confirmed that the oxide in the sample was Fe_3O_4 (Missana et al., 2003). Thermogravimetric analysis (TGA) with a heating rate of 10 °C min^{-1} in N_2 was used to investigate the deposition of Fe_3O_4 onto the surface of the GO platelets. The quantity of Fe_3O_4 deposited was determined based on the thermal stripping of oxygen-containing groups in the 200–500 °C temperature range (Fig. S2C) (Zhan et al., 2011). The quantity of Fe_3O_4 in MGO was approximately 25 wt%. The presence of Fe_3O_4 was also confirmed by Fourier transform infrared (FT-IR) spectroscopy (Fig. S2D). A characteristic peak for Fe_3O_4 was observed at 580 cm^{-1} and was attributed to the stretching mode of Fe–O (Zhan et al., 2011). X-ray diffraction patterns of NGPs, GO, Fe_3O_4 and MGO are shown in Fig. S3A and B (Liu et al., 2009). The introduction of

Please cite this article as: Lin, C.-W., et al., Biosensors and Bioelectronics (2014), http://dx.doi.org/10.1016/j.bios.2014.08.080

Fe_3O_4 resulted in XRD-detection of Fe_3O_4 peaks within MGO. The magnetization of MGO was 31 emu g^{-1}, compared to 0 emu g^{-1} for GO, as measured by a superconducting quantum interference device (SQUID) (Fig. S3C). This value was lower than the magnetization of 65 emu g^{-1} for pure Fe_3O_4 due to the proportional decrease in Fe_3O_4 per unit weight (Yang et al., 2013a). The magnetization of MGO was sufficient to avoid escape from the submerged electrode. It also allowed for the separation/isolation of plasma and the rapid construction of the sensor for electrochemical sensing in a magnetic field (Scheme 1B and C).

3.2. Studies of Avastin loading and optimal conditions

The loading efficiency of Avastin onto MGO was determined by colorimetric detection at a wavelength of 279 nm, which was chosen based on the absorption spectrum of unbound Avastin. The supernatants were measured after reacting MGO with various concentrations of Avastin. The optimal amount of Avastin immobilized on MGO was approximately 139.9 μg Avastin per mg of MGO (the grafting ratio was approximately 93.27%) (Fig. S4A). Optimal concentration of Avastin loading was 500 μg mL^{-1} (Fig. S4B). We further investigated the effect of the volume of Avastin-MGO pipetted onto the Au electrode (Fig. S4C). Finally, we investigated the effect of incubation time of VEGF (750 μg mL^{-1}) with the Avastin-MGO-modified Au electrode to determine the optimum time for producing a higher change in current (Fig. S4D). An increase in the VGEF incubation period resulted in an increase in the peak currents, which could be seen in the cyclic voltammograms. However, according to the results, there was no significant difference between the 30 and 120 min incubation periods (ΔI=4.82 μA and 5.08 μA for 30 and 120 min, respectively). Thus, to decrease the time for total VEGF immobilization and maintain the activity of VEGF, a 30 min incubation period was chosen. In summary, 15 μL Avastin-MGO (139.9 μg Avastin/mg MGO) was pipetted onto the Au electrode under a magnetic field to form the biosensor immediately, without requiring a drying step, and the sensor was incubated with VEGF for 30 min. The entire procedure was faster and more convenient than ELISA. The response time was reduced 10-fold compared with the ELISA method, which typically requires 5–5.5 h (Al-Ameen and Ghosh, 2013).

3.3. Electrochemical characterization of the Avastin-MGO-modified Au electrode

The electrochemical behavior of the Avastin-MGO-modified Au electrode was studied by cyclic voltammetry (CV) and differential pulse voltammetry (DPV) in a 1 mM ($K_3[Fe(CN)_6]$)/($K_4[Fe(CN)_6]$) /0.1 M KCl solution. The pH was maintained at 7.0 because the pH of blood samples was usually neutral, and all measurements were made at room temperature. In this study, using $K_4[Fe(CN)_6]/K_3[Fe(CN)_6]$ as the electro-active molecules provided a convenient and valuable approach for analyzing the electron transfer between the solution and the electrode surface, which occurs by tunneling through either the barrier of the interfaces or through defects in the barrier (Prabhulkar et al., 2009). We activate the Au electrode until two obvious peaks appeared at 0.55 and 0.78 V before a new electrode was used (Fig. S5). The cyclic voltammetry results showed almost completely reversible behavior on the bare Au electrode, the Avastin-MGO-modified Au electrode, and the Avastin-MGO-modified Au electrode treated with 1000 μg mL^{-1} VEGF from −0.2–0.6 V at a scan rate of 40 mV s^{-1} (Fig. 2A). However, the change observed in the voltammetric signal can be attributed

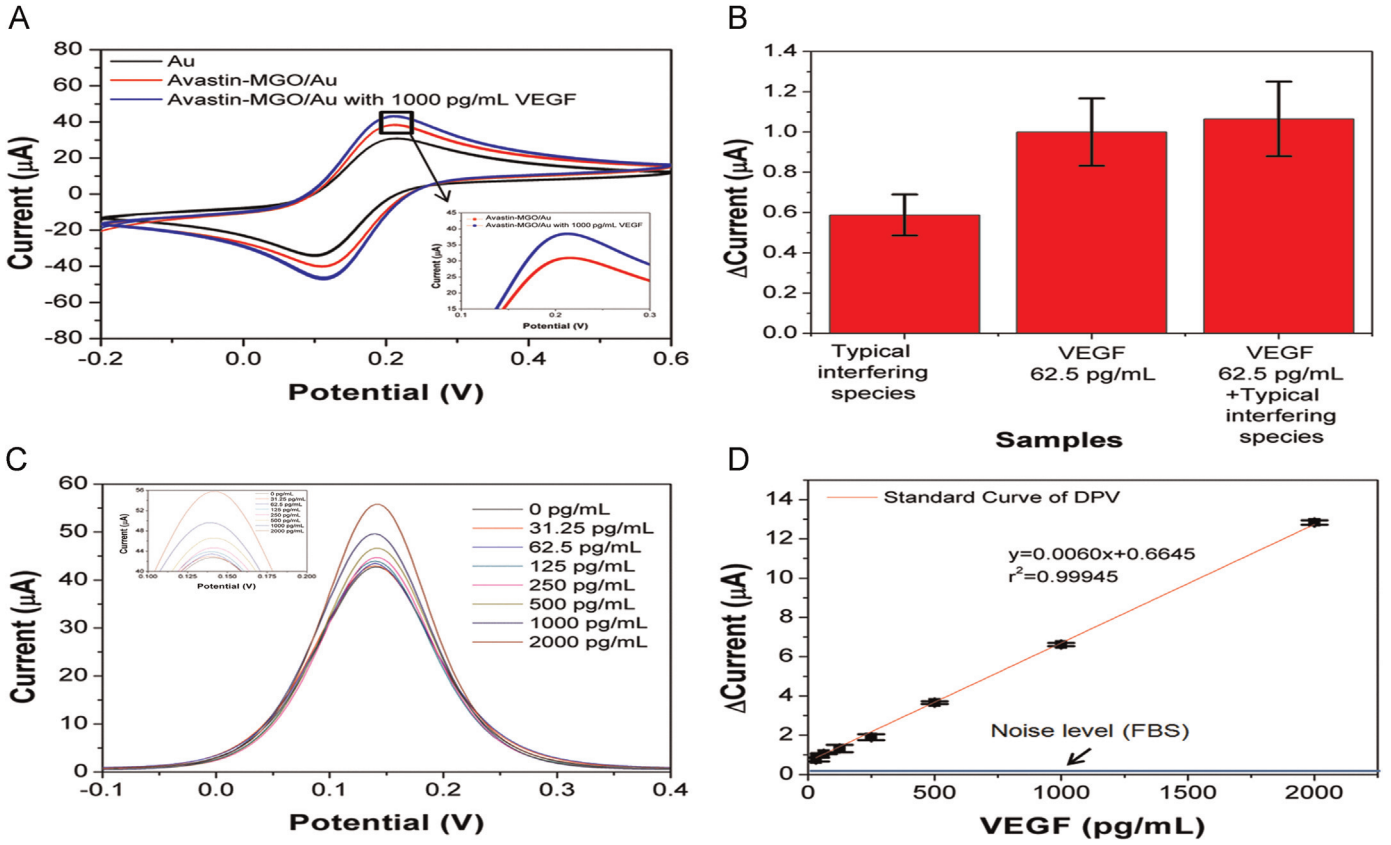

Fig. 2. (A) Cyclic voltammetry of Au (black), an Avastin-MGO-modified Au electrode (blue) and an Avastin-MGO-modified Au electrode combined with 1000 pg/mL^{-1} of VEGF (red). (B) Change in the current of various interference species (n=5). (C) DPV showing the increase in the electrochemical signal upon incubation of the electrode in samples with various concentrations of VEGF. (D) Calibration curve for the change in current (DPV) at different VEGF concentrations, measured by the Avastin-MGO-modified Au biosensor (n=5). (For interpretation of the references to color in this figure legend, the reader is referred to the web version of this article.)

to the effects of both steric blockage and charge repulsion/attraction effects (de la Escosura-Muñiz et al., 2013; Rodriguez et al., 2005). The increase in the voltammetric signal can be explained by considering the charge attraction effect. Avastin and VEGF are positively charged (Kaja et al., 2011; Vlckova et al., 2008), which produces an attraction to the negative charge of the $Fe(CN)_6{}^{-4}$ ions contained in the redox indicator. Thus, the ion diffusion to the electrode increased, and oxidation consequently increased, as shown in the inset of Fig. 2A. In this case, the charge effect between the redox indicator and the Avastin or VEGF was most likely a more important factor than steric blockage, which was minimal due to the relatively small size of the $[Fe(CN)_6]^{4-}$ ions diffusing to the electrode (de la Escosura-Muñiz et al., 2013). To further investigate the optimization of electrochemical, DPV scanning from −0.1 V to +0.4 V was performed to evaluate the oxidation signal of $[Fe(CN)_6]^{4-}$ to $[Fe(CN)_6]^{3-}$ at approximately +0.15 V.

3.4. Interference and performance of the Avastin-MGO-modified Au electrode

In the interference study, we incubated with typical interfering species in human plasma with the Avastin-MGO-modified Au electrode. The following interfering species were use: immunoglobulin G (IgG, 1000 ng dL^{-1}), immunoglobulin M (IgM, 192.5 mg dL^{-1}), glucose (5 mM), ascorbic acid (AA, 4.3 μg mL^{-1}), and uric acid (UA, 0.295 mM) (Khan et al., 2011; Marquette et al., 2003). The results were evaluated based on the change in current with the addition of VEGF. Additional washing with DI water was performed after hybridization, prior to measurement, to eliminate the influence of free VEGF and other interfering species in the serum (Fig. 2B). No significant current changes were detected for the addition of the typical interfering species (0.59 ± 0.10 μA). Furthermore, the change in current after the addition of VEGF in the presence of the interfering species (1.065 ± 0.19 μA for 62.5 pg mL^{-1}) was not different compared to treatment with 62.5 pg mL^{-1} VEGF alone (1.0 ± 0.17 μA). Thus, the Avastin-MGO-modified Au sensor resisted interference well.

The change in current (ΔC) generated by ferricyanide ($[Fe(CN)_6]^{3-/4-}$) was also measured by differential pulse voltammetry (DPV), which eliminates capacitive and non-Faradaic currents in the scan, thus increasing sensitivity (Moscovici et al., 2013). Before VEGF capture, the sensor displayed a peak current of 42.7 μA at 0.14 V, which corresponded to the redox reaction between $[Fe(CN)_6]^{3-/4-}$ and the sensor surface. The current signals measured for VEGF target proteins at various concentrations (31.25, 62.5, 125, 250, 500, 1000, 2000 pg mL^{-1}) using the fabricated electrochemical immunosensor were obtained under optimized conditions (Fig. 2C). The current increased with increasing VEGF concentration, presumably due to depletion of charge carriers in the Au electrode as more positively charged VEGF molecules bound to the Avastin-functionalized surface (Rodriguez et al., 2005; Vlckova et al., 2008). The change in the oxidation peak current as a function of VEGF concentration is shown in the inset of Fig. 2C. Here, ΔC increased linearly with increasing VEGF concentrations from 31.25 pg mL^{-1} to 2000 pg mL^{-1}, indicating that the response was the direct result of VEGF binding to the Avastin-MGO through antigen–antibody recognition (Fig. 2D). Furthermore, various VEGF concentrations were evaluated in the presence of the interfering species described above. Although these values reflected the presence of interfering species, the variations were insignificant. The lowest VEGF concentration (31.25 pg mL^{-1}) produced a 0.76 ± 0.10 μA current change, which was differentiated from the noise level (a 0.20 ± 0.06 μA current change, $n=6$) resulting from the fetal bovine serum (FBS). From this result, the limit of detection (L.O.D) was found to be 31.25 pg mL^{-1}. This level is slightly higher than the value measured by ELISA (6.4 pg mL^{-1}) (Al-Ameen and Ghosh, 2013). However, it is still better than for other reported electrochemical (Kim et al., 2010; Prabhulkar et al., 2009; Zhao et al., 2011) and optical biosensors for VEGF (Al-Ameen and Ghosh, 2013; Chen et al., 2013) because of the lower L.O.D and wider detection range. In addition, these clinically relevant levels of VEGF which already were reported were inside in our detection range (Kut et al., 2007). In summary, these results suggest that our detection system can provide a simple, cheap, stable, reusable, fast, highly selective and sensitive amperometric assay platform for future clinical diagnosis.

3.5. Determination of VEGF in human plasma

VEGF is an important biomarker for cancer growth and is often overexpressed in tumors (Barton et al., 1997; Kido et al., 2001). Furthermore, patients with various tumors typically have higher VEGF concentrations in their plasma than healthy individuals (Kaya et al., 2004; Kido et al., 2001; Poon et al., 2003; Ugurel et al., 2001). A high concentration of VEGF in the serum and tumor tissue of brain tumor patients was previously reported (Takano et al., 1996). Increased VEGF concentration also has a high correlation with tumor progression and survival in malignant melanoma patients (Ugurel et al., 2001). In this study, serum samples were collected from healthy people ($n=2$) and patients ($n=4$) diagnosed with low stages of brain tumor to assess the utility of the Avastin-MGO-modified Au electrode-based VEGF biosensor for clinical analysis. We compared our sensing system to the conventional detection of VEGF by ELISA using the human serum samples. The concentrations of VEGF were calculated using calibration curves for the electrochemical sensing and ELISA assays (Figs. 2D and S6). The concentrations of VEGF in the serum of healthy people measured by our electrochemical biosensor were relatively low (49.81 ± 2.55 pg mL^{-1} and 64.25 ± 17.64 pg mL^{-1}) compared to the brain tumor patients' serum samples (167.58 ± 18.33 pg mL^{-1}, 143.69 ± 12.62 pg mL^{-1}, 177.03 ± 30.75 pg mL^{-1} and 196.47 ± 22.19 pg mL^{-1}) (Fig. 3B). These raw data were showed and compared with the result by ELISA method in Table S1. According to past researches (Li et al., 2004), VEGF level of healthy people usually is defined lower 100 pg/mL, and VEGF levels are obviously increase by progress of clinical stage (stage I–II

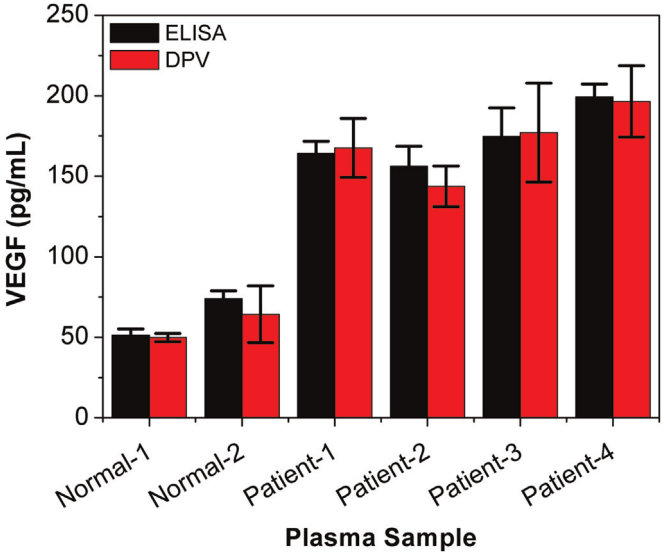

Fig. 3. Plasma VEGF concentrations measured by the Avastin-MGO-modified Au biosensor and an ELISA ($n=3$).

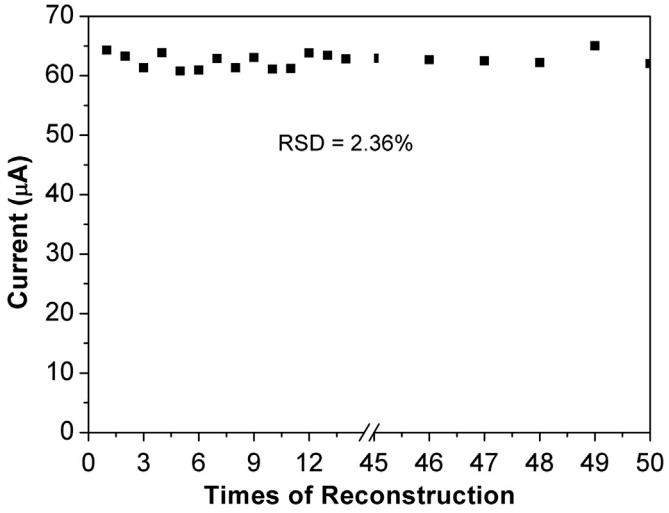

Fig. 4. Reusability of the Avastin-MGO-modified Au biosensor. The sensor showed no decrease in function after 50 times of reconstruction (RSD=2.36%).

198 pg mL^{-1}; stage III–IV 955 pg mL^{-1}) in ovarian cancer. Besides, similar VEGF values were reported by another research team (Sciacca et al., 2004), indicating that VEGF is overexpressed in patients suffering brain tumors. Meanwhile, the values obtained with our electrochemical biosensor were not significantly different from those measured by ELISA. This result suggests that our biosensor was capable of reliable, highly selective, rapid and accurate detection of VEGF in human serum for cancer diagnosis.

3.6. *Reusability and reproducibility*

Another advantage of this platform is that the sensor can be quickly reconstructed by washing out the deposited Avastin-MGO and pipetting additional Avastin-MGO solution (15 μL) onto the detection area of the same magnetic Au electrode (Scheme 1B) under optimized conditions. After reconstructing the sensor 50 times by depositing the same amount of Avastin-MGO solution, the current remained in the range of 59.24–65.03 μA (Fig. 4). This result confirmed the good reusability of the Au electrode and the stable covering process of the Avastin-MGO solution. The relative responses indicated a good relative standard deviation (RSD) of 2.36%. Therefore, the reusability of the sensor was also tested to show that the Pt electrode could be reused. Thus, the result proved the Au electrode could be reused at least 50 times.

4. Conclusion

In summary, we developed a simple method using DPV for the detection of VEGF isolated on an Avastin-MGO-modified Au biosensor. This biosensor can be used to detect VEGF in plasma samples. Furthermore, the Avastin-MGO solution can be drop-deposited onto the surface of a Au electrode in a magnetic field to quickly fabricate the biosensor for subsequent catalytically based detection of VEGF, and the biosensor showed good stability (RSD=2.36%, $n=50$). The lowest detectable concentration of VEGF was 31.25 pg mL^{-1}, and the amount of VEGF detected was close to that measured by an ELISA. Our study provides a broad and suitable working range that is comparable to ELISA methods. In addition, it simultaneously provides high specificity, re-usability, stability, and low cost, as well as a 10-fold reduction in the response time for the rapid detection of VEGF in cancer diagnosis. Thus, this study presents the groundwork for the utilization of MGO and Avastin in medical diagnostics and biotechnology.

Acknowledgments

We thank the Chang Gung Memorial Hospital, (NHRI-EX103-10004NI, CMRPG3D0571, CMRPG3D1111) and National Tsing Hua University (103A0045J2, 103N2753E1) for financial support. We also thank the Boost Program from the Low Carbon Energy Research Center of National Tsing Hua University and the Chang Gung Memorial Hospital Microscopy Core Laboratory.

Appendix A. Supplementary information

Supplementary data associated with this article can be found in the online version at http://dx.doi.org/10.1016/j.bios.2014.08.080.

References

Al-Ameen, M.A., Ghosh, G., 2013. Biosens. Bioelectron. 49, 105–110.
Aoyagi, K., Kouhuji, K., Yano, S., Miyagi, M., Imaizumi, T., Takeda, J., Shirouzu, K., 2005. Gastric Cancer 8 (3), 155–163.
Bando, H., Brokelmann, M., Toi, M., Alitalo, K., Sleeman, J.P., Sipos, B., Gröne, H.-J., Weich, H.A., 2004. Int. J. Cancer 111 (2), 184–191.
Barton, D.P., Cai, A., Wendt, K., Young, M., Gamero, A., De Cesare, S., 1997. Clin. Cancer Res. 3 (9), 1579–1586.
Carmeliet, P., Jain, R.K., 2000. Nature 407 (6801), 249–257.
Chen, Z., Lei, Y., Gao, W., Liu, J., 2013. Plasmonics 8 (2), 605–611.
Cheng, S.Y., Huang, H.J., Nagane, M., Ji, X.D., Wang, D., Shih, C.C., Arap, W., Huang, C. M., Cavenee, W.K., 1996. Proc. Natl. Acad. Sci. USA 93 (16), 8502–8507.
Clark, L.C., Lyons, C., 1962. Ann. NY Acad. Sci. 102 (1), 29–45.
de la Escosura-Muñiz, A., Chunglok, W., Surareungchai, W., Merkoçi, A., 2013. Biosens. Bioelectron. 40 (1), 24–31.
Ferrara, N., Gerber, H.-P., LeCouter, J., 2003. Nat. Med. 9 (6), 669–676.
Hanahan, D., Folkman, J., 1996. Cell 86 (3), 353–364.
Hsu, M.Y., Yang, C.Y., Hsu, W.H., Lin, K.H., Wang, C.Y., Shen, Y.C., Chen, Y.C., Chau, S.F., Tsai, H.Y., Cheng, C.M., 2014. Biomaterials 35 (12), 3729–3735.
Jain, R.K., 2003. Nat. Med. 9 (6), 685–693.
Kaja, S., Hilgenberg, J.D., Everett, E., Olitsky, S.E., Gossage, J., Koulen, P., 2011. Hum. Antib. 20 (3–4), 95–101.
Kauffmann, J.M., Guilbault, G.G., 1991. Bioprocess Technol. 15, 63–82.
Kaya, A., Çiledag, A., Gulbay, B.E., Poyraz, B.M., Çelik, G., Sen, E., Savas, H., Savas, I., 2004. Respir. Med. 98 (7), 632–636.
Khan, A., Khan, M.I., Iqbal, Z., Shah, Y., Ahmad, L., Nazir, S., Watson, D.G., Khan, J.A., Nasir, F., Khan, A., Ismail, 2011. Talanta 84 (3), 789–801.
Kido, S., Kitadai, Y., Hattori, N., Haruma, K., Kido, T., Ohta, M., Tanaka, S., Yoshihara, M., Sumii, K., Ohmoto, Y., Chayama, K., 2001. Eur. J. Cancer 37 (12), 1482–1487.
Kim, G.-I., Kim, K.-W., Oh, M.-K., Sung, Y.-M., 2010. Biosens. Bioelectron. 25 (7), 1717–1722.
Kuila, T., Bose, S., Khanra, P., Mishra, A.K., Kim, N.H., Lee, J.H., 2011. Biosens. Bioelectron. 26 (12), 4637–4648.
Kut, C., Mac Gabhann, F., Popel, A.S., 2007. Br. J. Cancer 97 (7), 978–985.
Kwon, O.S., Park, S.J., Jang, J., 2010. Biomaterials 31 (17), 4740–4747.
Laguens, G., Coronato, S., Girolamo, W.D., 2006. Cent. Eur. J. Med. 1 (4), 330–347.
Li, L., Wang, L., Zhang, W., Tang, B., Zhang, J., Song, H., Yao, D., Tang, Y., Chen, X., Yang, Z., Wang, G., Li, X., Zhao, J., Ding, H., Reed, E., Li, Q.Q., 2004. Anticancer Res. 24 (3b), 1973–1979.
Li, S.-M., Yang, S.-Y., Wang, Y.-S., Lien, C.-H., Tien, H.-W., Hsiao, S.-T., Liao, W.-H., Tsai, H.-P., Chang, C.-L., Ma, C.-C.M., Hu, C.-C., 2013. Carbon 59, 418–429.
Liu, Y., Jiang, W., Li, S., Li, F., 2009. Appl. Surf. Sci. 255 (18), 7999–8002.
Lu, Y.J., Yang, H.W., Hung, S.C., Huang, C.Y., Li, S.M., Ma, C.C., Chen, P.Y., Tsai, H.C., Wei, K.C., Chen, J.P., 2012. Int. J. Nanomed. 7, 1737–1747.
Marquette, C.A., Degiuli, A., Blum, L., amp, x, c, J., 2003. Biosens. Bioelectron. 19 (5), 433–439.
Missana, T., Maffiotte, C., García-Gutiérrez, M., 2003. J. Colloid Interface Sci. 261 (1), 154–160.
Moscovici, M., Bhimji, A., Kelley, S.O., 2013. Lab Chip 13 (5), 940–946.
Poon, R.T.-P., Lau, C.P.-Y., Cheung, S.-T., Yu, W.-C., Fan, S.-T., 2003. Cancer Res. 63 (12), 3121–3126.
Prabhulkar, S., Alwarappan, S., Liu, G., Li, C.-Z., 2009. Biosens. Bioelectron. 24 (12), 3524–3530.
Rodriguez, M.C., Kawde, A.N., Wang, J., 2005. Chem. Commun. 34, 4267–4269.
Sciacca, F.L., Ciusani, E., Silvani, A., Corsini, E., Frigerio, S., Pogliani, S., Parati, E., Croci, D., Boiardi, A., Salmaggi, A., 2004. Clin. Cancer Res. 10 (4), 1312–1317.
Stankovich, S., Dikin, D.A., Dommett, G.H.B., Kohlhaas, K.M., Zimney, E.J., Stach, E.A., Piner, R.D., Nguyen, S.T., Ruoff, R.S., 2006. Nature 442 (7100), 282–286.
Stankovich, S., Dikin, D.A., Piner, R.D., Kohlhaas, K.A., Kleinhammes, A., Jia, Y., Wu, Y., Nguyen, S.T., Ruoff, R.S., 2007. Carbon 45 (7), 1558–1565.
Takano, S., Yoshii, Y., Kondo, S., Suzuki, H., Maruno, T., Shirai, S., Nose, T., 1996. Cancer Res. 56 (9), 2185–2190.
Teymourian, H., Salimi, A., Khezrian, S., 2013. Biosens. Bioelectron. 49, 1–8.

Ugurel, S., Rappl, G., Tilgen, W., Reinhold, U., 2001. J. Clin. Oncol. 19 (2), 577–583.
Vlckova, M., Kalman, F., Schwarz, M.A., 2008. J. Chromatogr. A 1181 (1–2), 145–152.
Wang, Y., Fei, D., Vanderlaan, M., Song, A., 2004. Angiogenesis 7 (4), 335–345.
Wu, H., Huang, C., Chang, D., 2008. J. Cancer Mol. 4, 37–45.
Wu, W., Shu, X., Hovsepyan, H., Mosteller, R.D., Broek, D., 2003. Oncogene 22 (22), 3361–3370.
Yang, H.-W., Hua, M.-Y., Chen, S.-L., Tsai, R.-Y., 2013a. Biosens. Bioelectron. 41, 172–179.
Yang, H.-W., Hua, M.-Y., Hwang, T.-L., Lin, K.-J., Huang, C.-Y., Tsai, R.-Y., Ma, C.-C.M., Hsu, P.-H., Wey, S.-P., Hsu, P.-W., Chen, P.-Y., Huang, Y.-C., Lu, Y.-J., Yen, T.-C., Feng, L.-Y., Lin, C.-W., Liu, H.-L., Wei, K.-C., 2013b. Adv. Mater. 25 (26), 3605–3611.
Yang, H.-W., Lu, Y.-J., Lin, K.-J., Hsu, S.-C., Huang, C.-Y., She, S.-H., Liu, H.-L., Lin, C.-W., Xiao, M.-C., Wey, S.-P., Chen, P.-Y., Yen, T.-C., Wei, K.-C., Ma, C.-C.M., 2013c. Biomaterials 34 (29), 7204–7214.
Yang, S.-Y., Chang, K.-H., Tien, H.-W., Lee, Y.-F., Li, S.-M., Wang, Y.-S., Wang, J.-Y., Ma, C.-C.M., Hu, C.-C., 2011. J. Mater. Chem. 21 (7), 2374–2380.
Zhan, Y., Meng, F., Yang, X., Liu, X., 2011. Colloids Surf. A: Physicochem. Eng. Asp. 390 (1–3), 112–119.
Zhang, B., Iezzi, R., Cui, T., 2013. In: Proceedings of the 17th International Conference on Solid-State Sensors, Actuators and Microsystems (TRANSDUCERS & EUROSENSORS XXVII), pp. 143-146.
Zhao, S., Yang, W., Lai, R.Y., 2011. Biosens. Bioelectron. 26 (5), 2442–2447.

Please cite this article as: Lin, C.-W., et al., Biosensors and Bioelectronics (2014), http://dx.doi.org/10.1016/j.bios.2014.08.080